Nonlinear Image Restoration in Confocal Microscopy *

J.B.T.M. Roerdink
Dept. of Computing Science, University of Groningen
P.O. Box 800, 9700 AV Groningen, The Netherlands
Tel. +31-50-633931; Fax +31-50-633800; Email roe@cs.rug.nl

1 Introduction

A major problem in 3D imaging by a CSLM (confocal scanning laser microscope) in the (epi)fluorescence mode is the darkening of the deeper layers due to scattering and absorption of excitation and fluorescence light. In [2] we developed a new restoration method, called the 'FFT-method', to correct for these effects by deriving a correction factor to the standard restoration in the form of a 3D convolution of the measured signal, which can be efficiently computed by the use of the Fast Fourier Transform (FFT). In this way, the complexity of computation is reduced to $\mathcal{O}(N_z \log N_z)$, where N_z is the number of vertical layers. We also compared the computational efficiency of our algorithm with the iterative layer method 'with condensation' developed in [4], which has complexity $\mathcal{O}(N_z^2)$. For spatially varying image densities the restoration quality using our method was found to be a little poorer than in the layer method.

This paper gives a succinct summary of an extension to this approach as published in [3]. There it is shown that the accuracy of the FFT-method can be improved by first order moment and cumulant estimators leading to a nonlinear integral equation for the unknown fluorescent density, which is solved by an iterative method. The new estimators, the moment estimator in particular, are more accurate than the layer method. Since the computations involve only discrete 3D convolutions computable by the FFT, the advantage in computational efficiency over the layer method is retained.

2 The CSLM transform

When a CSLM is operating in the fluorescence mode a laser beam is focussed upon a point $\mathbf{r} = (x, y, z)$ in the object, see Fig. 1. Here the z-direction is chosen along the optical axis. The rays converging to the object point are contained in a 'light cone' with angle ω, called the 'semi-aperture angle'. The radiation absorbed at the point in focus is uniformly reemitted as fluorescent radiation and the part which travels back the same route as the incoming radiation is detected. While travelling through the sample the radiation is attenuated with an attenuation factor which is spatially dependent. Then, assuming that (i) the attenuation of the excitation light equals that of the fluorescence light, and (ii) that this attenuation coefficient is proportional to the (unknown) fluorescent density $\rho(\mathbf{r})$, one can derive the following nonlinear integral transform ('CSLM-transform'):

$$f(\mathbf{r}) = \rho(\mathbf{r}) \times \gamma_f(\mathbf{r})\gamma_b(\mathbf{r}), \tag{1}$$

Here $f(\mathbf{r})$ is the measured fluorescent intensity,

$$\gamma_f(\mathbf{r}) := C_f \int_0^{\omega} d\theta \int_0^{2\pi} d\phi \ \sin\theta \ \cos\theta \ \exp\left[-\varepsilon \int_0^z \frac{dz'}{\cos\theta} \ \rho(\hat{\mathbf{r}})\right] \tag{2}$$

is the forward attenuation factor, and

$$\gamma_b(\mathbf{r}) := C_b \int_0^{\omega} d\theta \int_0^{2\pi} d\phi \ \sin\theta \ \exp\left[-\varepsilon \int_0^z \frac{dz'}{\cos\theta} \ \rho(\hat{\mathbf{r}})\right] \tag{3}$$

*In: Proc. Computing Science in the Netherlands, 21-22 november, Utrecht, 1994, pp. 253-259. Postscript version obtainable at http://www.cs.rug.nl/~roe/.

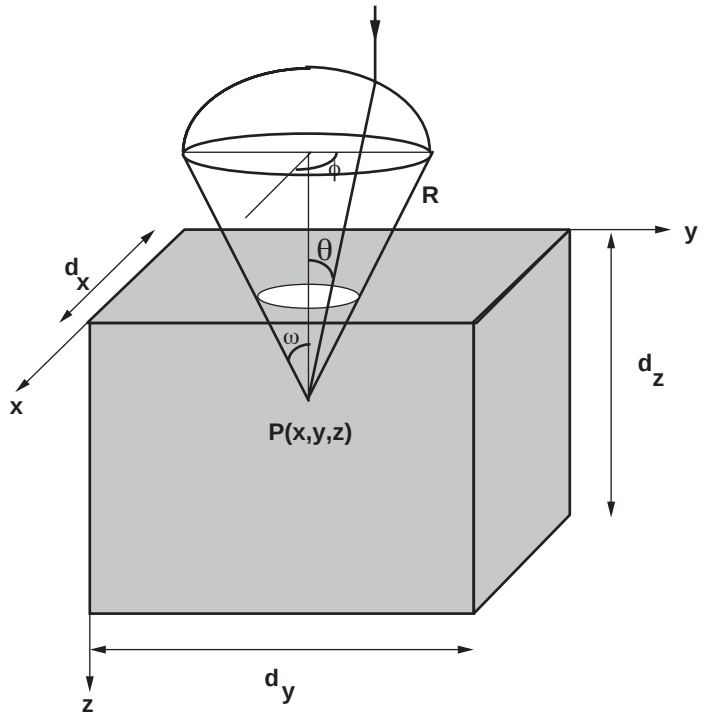

FIGURE 1: *CSLM geometry of light cone with apex at a point $P(x, y, z)$ in the object. R: radius of spherical bundle; ω: semi-aperture angle; (θ, ϕ): polar angles of light ray; d_z: depth of the sample. The optical axis coincides with the z-axis.*

is the backward attenuation factor. In these equations ε is a proportionality constant and C_f and C_b are normalization constants. Here $\hat{\mathbf{r}}$ is the vector

$$\hat{\mathbf{r}}(\mathbf{r}; \theta, \phi, z') = (x + (z - z') \tan\theta \cos\phi,\ y + (z - z') \tan\theta \sin\phi,\ z'). \tag{4}$$

The quantity $\varepsilon\, d_z$ is a measure for the degree of attenuation, where d_z is the depth of the sample.

Inversion of the CSLM transform

By a perturbation expansion in the parameter ε, which is tantamount to the assumption of weak attenuation, we derived in [2] the following approximation $\tilde{\rho}(\mathbf{r})$ for the fluorescent density,

$$\tilde{\rho}(\mathbf{r}) = f(\mathbf{r}) \{1 + \varepsilon\ c(\mathbf{r})\}, \tag{5}$$

where $c(\mathbf{r})$ is the convolution integral

$$c(\mathbf{r}) = \int_{-\infty}^{\infty} \int_{-\infty}^{\infty} \int_{-\infty}^{\infty} d\mathbf{r}'\ \kappa(\mathbf{r}')\ f(\mathbf{r} - \mathbf{r}'), \tag{6}$$

with $\kappa(\mathbf{r})$ the space-invariant kernel given by

$$\kappa(x, y, z) = \begin{cases} C_f \frac{z}{(x^2+y^2+z^2)^{3/2}} + C_b \frac{1}{x^2+y^2+z^2}, & 0 \le z \le d_z,\ x^2 + y^2 \le (z \tan\omega)^2 \\ 0 & \text{elsewhere} \end{cases}. \tag{7}$$

Numerical computation

For numerical computation, the integral (6) is discretized on a grid of $N_x \times N_y \times N_z$ voxels, each voxel being a box of dimensions $\delta_x, \delta_y, \delta_z$ in the x-, y- and z-directions. Then the approximation (5) is replaced by

$$R_{ijk} = F_{ijk}(1 + \varepsilon\ C_{ijk}), \tag{8}$$

where

$$C_{ijk} = \sum_{i'=-\frac{M_x}{2}+1}^{\frac{M_x}{2}} \sum_{j'=-\frac{M_y}{2}+1}^{\frac{M_y}{2}} \sum_{k'=1}^{M_z} K_{i'j'k'}\ F_{i-i',j-j',k-k'}, \tag{9}$$

with $R_{ijk}, C_{ijk}, K_{ijk}$ and F_{ijk} the discrete counterparts of $\tilde{\rho}(x,y,z), c(x,y,z), \kappa(x,y,z)$ and $f(x,y,z)$, respectively, with (i,j,k) in the index set $I\!I := \{(i,j,k) : i = 1,..,N_x;\ j = 1,..,N_y;\ k = 1,..,N_z\}$, and array elements are defined to be zero when the indices are not in the index set $I\!I$. The discrete convolution (9) can be computed efficiently by FFT methods [2].

3 Iterative algorithms

By applying moment and cumulant expansions of characteristic functions [3] one obtains equations for the 'moment approximation' $\rho^{(m)}(\mathbf{r})$ and the 'cumulant approximation' $\rho^{(c)})(\mathbf{r})$ in the form

$$\rho^{(c)}(\mathbf{r}) = f(\mathbf{r}) \exp\left[\varepsilon\ (\kappa * \rho^{(c)})(\mathbf{r})\right], \tag{10}$$

and

$$\rho^{(m)}(\mathbf{r}) = f(\mathbf{r}) \left[1 - \varepsilon\ (\kappa * \rho^{(m)})(\mathbf{r})\right]^{-1}, \tag{11}$$

where $\kappa * \rho^{(\beta)}$ denotes the convolution of the functions κ and $\rho^{(\beta)}$, $\beta = m, c$, and the kernel κ is identical to that in (7). We assume that ε is chosen small enough for the inverse in (11) to exist.

After discretization, both (10) and (11) lead to a finite system of nonlinear equations of the form

$$R_{ijk} = F_{ijk}\ G\Big((K * R)_{ijk}\Big), \qquad (i,j,k) \in I\!I, \tag{12}$$

where $G(x) = \exp(\varepsilon x)$ for the cumulant approximation and $G(x) = (1 - \varepsilon x)^{-1}$ for the moment approximation, respectively, with $K * R$ the discrete convolution of the 3D arrays K and R.

The equations (12) can be solved by Picard iteration [1], with F_{ijk} as the initial estimate:

$$R^{(0)}_{ijk} = F_{ijk}, \tag{13}$$

$$R^{(n)}_{ijk} = F_{ijk}\ G\left((K * R^{(n-1)})_{ijk}\right), \qquad n = 1, 2, 3, \ldots . \tag{14}$$

Each iteration step involves the computation of the discrete convolution $K * R^{(n-1)}$ of the estimate $R^{(n-1)}$ of the previous iteration (with the same convolution kernel K) which can be efficiently computed by the FFT. The first iterate of Eq. 14 with $G(x) = 1 + \varepsilon x$ coincides with the discrete analogon of Eq. 5 and is the approximation used in [2].

It can be shown that (for proofs, see [3]):

- The equations (12) have a unique solution;
- The iterates $R^{(n)}_{ijk}$ of Eq. 14 converge in a finite number of N_z steps towards the unique solution of Eq. 12;
- The convergence is monotonous, that is, $R^{(n)}_{ijk} \geq R^{(n-1)}_{ijk}$;
- The estimators $\rho^{(m)}$ and $\rho^{(c)}$ satisfy the inequality

$$\rho^{(c)} \leq \rho^{(m)}. \tag{15}$$

The restoration procedure

The complete procedure of reconstructing the fluorescent density from measured data contains the following steps:

1. Read the measured data $F_{ijk}, i = 1,..,N_x, j = 1,..,N_y, k = 1,..,N_z$.
2. Determine the appropriate value of the attenuation constant ε.

3. Iteratively compute

$$R_{ijk}^{(n)} = F_{ijk}\ G\left((K * R^{(n-1)})_{ijk}\right), \qquad n = 1, 2, 3, ..., \tag{16}$$

where $R_{ijk}^{(0)} = F_{ijk}$, and $G(x) = (1 - \varepsilon x)^{-1}$ or $G(x) = \exp(\varepsilon x)$ for the moment and cumulant estimator, respectively.

In each iteration the convolution of the previous estimate is computed by means of the FFT (using the same kernel K as defined above).

Input parameters of the algorithm are the dimensions N_x, N_y, N_z of the data array, the scanning steps $\delta_x, \delta_y, \delta_z$, the semi-aperture angle ω and the attenuation constant ε. For the determination of the correct value of ε one may resort to a calibration experiment in which a homogeneous test sample is used [4]. In this paper we will consider test densities for which the value of ε is known.

4 Restoration of a test image

In this section we consider a test image consisting of a number of circles and ellipses already used in [2]. Signal data F_{ijk} were generated by numerically computing the integrals in (2)–(3) for a number of equidistant 3D positions. The parameters were chosen as follows: $d_x = d_y = 1.0, d_z = 0.1$, $N_x = N_y = 128$, $N_z = 8$, $\omega = 1.04719$. We computed the relative root mean square error

$$\mathrm{E}(z) := \left(\frac{\sum_{x=1}^{N_x} \sum_{y=1}^{N_y} \{\rho(x,y,z) - \tilde{\rho}(x,y,z)\}^2}{\sum_{x=1}^{N_x} \sum_{y=1}^{N_y} \{\rho(x,y,z)\}^2} \right)^{\frac{1}{2}},$$

between original density ρ and restored density $\tilde{\rho}$ at each plane $z = constant$. Computations were performed on a SPARC workstation (35 Mhz, 26 MIPS), taking about one minute per iteration step.

εz	signal error	iter = 1	iter = 2	iter = 3
0.0000	0.000	0.000	0.000	0.000
0.0625	0.116	0.004	0.004	0.004
0.1250	0.218	0.006	0.016	0.016
0.1875	0.305	0.025	0.041	0.045
0.2500	0.382	0.065	0.065	0.090
0.3125	0.450	0.127	0.075	0.153
0.3750	0.509	0.200	0.056	0.236
0.4375	0.560	0.278	0.026	0.330

TABLE 1: *Signal error and restoration errors by the moment estimator $\rho^{(m)}$ after one, two and three iterations as a function of the effective depth εz.*

εz	signal error	iter = 1	iter = 2	iter = 3
0.0000	0.000	0.000	0.000	0.000
0.0625	0.116	0.010	0.010	0.010
0.1250	0.218	0.035	0.022	0.022
0.1875	0.305	0.080	0.047	0.046
0.2500	0.382	0.141	0.089	0.084
0.3125	0.450	0.213	0.146	0.136
0.3750	0.509	0.286	0.213	0.198
0.4375	0.560	0.357	0.283	0.265

TABLE 2: *Signal error and restoration errors by the cumulant estimator $\rho^{(c)}$ after one, two and three iterations as a function of the effective depth εz.*

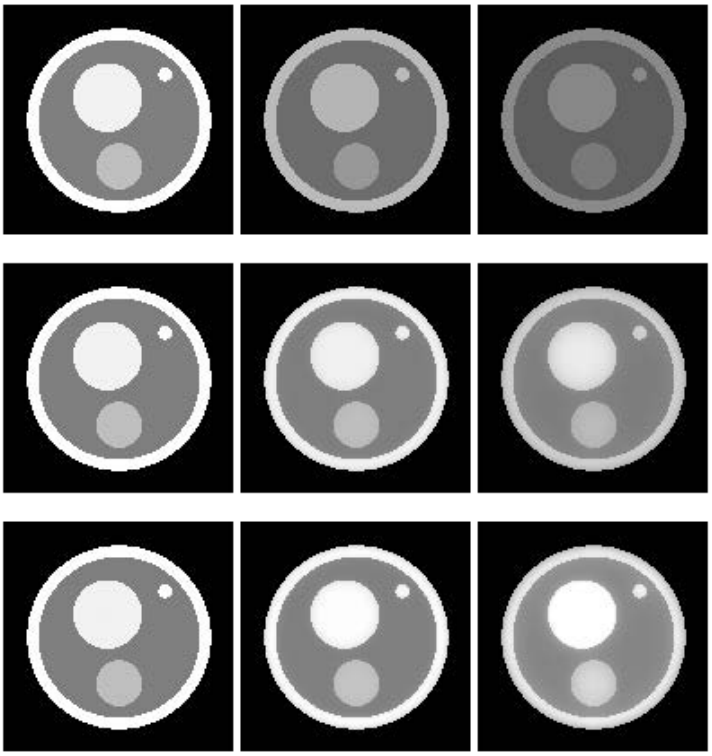

FIGURE 2: *Restoration of the circle image. First row: the attenuated test images; second row: restoration by the cumulant estimator (iter = 2); third row: restoration by the moment estimator (iter = 2). In each row, the first, fourth and seventh layer is displayed from left to right. The original image in each layer is identical to the first image in row 1.*

Results are shown in Table 1 for the moment estimator (11) and in Table 2 for the cumulant estimator (10). In the case of the moment estimator the errors first decrease and then start to grow again after the second iteration. This is due to the fact that the initial estimate $f(\mathbf{r})$ is smaller then the exact density $\rho(\mathbf{r})$, so that at first the iterates underestimate the true solution. Because of the monotonicity property mentioned in Section 3 the iterates always increase so that (if the solution $\rho^{(m)}$ is larger than the true ρ, which is apparently the case here) they will start to overestimate the true density. The cumulant estimator $\rho^{(c)}$ underestimates the true density, and the values were stable within an accuracy of three digits after the third iteration. For comparison we give in column 2 of the Tables the error *before* restoration, denoted by 'signal error' and computed according to (4) with $\tilde{\rho}$ replaced by f.

Comparing with the numbers in Table 4 of [2], we conclude that both the moment estimator with $iter = 1, 2$ and cumulant estimator with $iter \geq 2$ are more accurate than the layer method of [4] which gives a restoration error of 0.301 at the deepest layer. From the Tables it is clear that the moment estimator, when run to convergence, overestimates the exact image densities. The first iterate, however, underestimates the exact values. Therefore, in case of the moment estimator, we take the reconstruction corresponding to the intermediate value $iter = 2$, which gives the best results. In Fig. 2 we show the corresponding restored images. We rescale the values of the densities to make sure that they occupy the complete grey-scale, which consists of the set of integer values from 0 to 255. In order to avoid that a few outliers cause a large visual degradation of the resulting images, we constrained the approximate solutions $\tilde{\rho}$ to lie between the known lower and upper bounds, i.e. $0 \leq \tilde{\rho} \leq 1$. In each row, the first, fourth and seventh layer is displayed from left to right, out of a total of 8 depth layers. Since the exact density $\rho(\mathbf{r})$ does not depend on z, the original image in each layer is identical to the first image in row 1. The first row contains the attenuated test images $f(\mathbf{r})$, the second row the restoration by the cumulant estimator and the third row the restoration by the moment estimator, both after two iterations. The images which are restored by the cumulant estimator are virtually identical to those of the layer method of Visser et al.

[4], cf. Figure 4 of [2]. Clearly the largest improvement in restoration quality has been obtained by using the moment estimator. The reconstruction is not perfect, however: the central regions in the centers of the light circular regions are slightly overestimated. The calculations have been repeated for other test images, leading to similar conclusions: the reconstruction errors are smallest when using the moment estimator with $iter = 2$, but the reconstructed images still show some differences when compared to the original images, see [3]. Nevertheless, a considerable improvement in restoration accuracy has been obtained by using the estimators developed here, which in addition are efficiently computable by using FFT methods.

5 Restoration of a real CSLM image

The method of this paper was applied to a CSLM image ($N_x = N_y = 256$, $N_z = 8$) of a geological sample consisting of sandstone cavities filled with a fluorescent oily substance, also considered in [4] and [2]. The result is shown in Fig. 3. Again the best result is obtained by the moment estimator, which shows substantially more detail than the original image. This shows the practical usefulness of the method. We determined the value of ε in this case so as to give a visually satisfactory restoration.

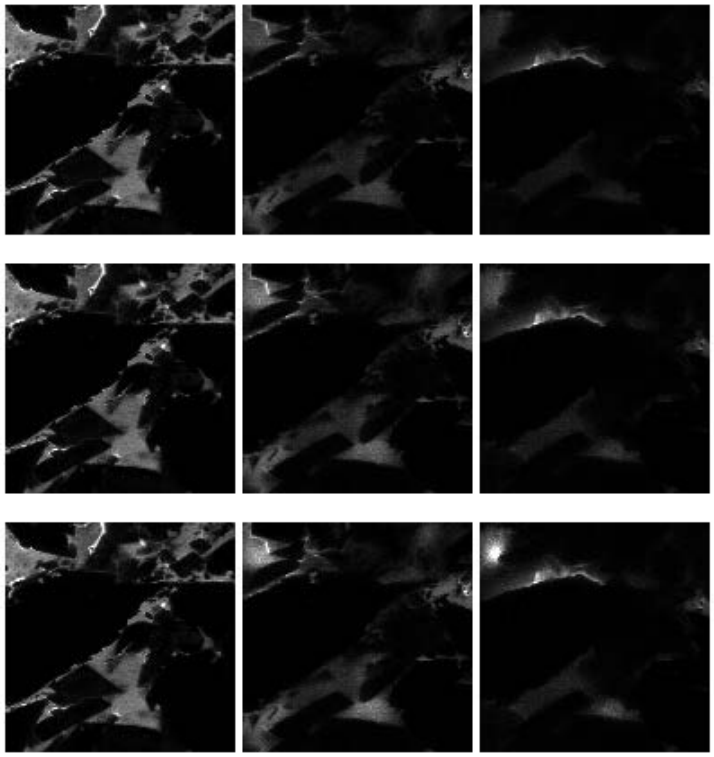

FIGURE 3: *Restoration of the sandstone CSLM image. First row: the attenuated CSLM images; second row: restoration by the cumulant estimator (iter = 2); third row: restoration by the moment estimator (iter = 2). In each row, the first, fourth and seventh layer is displayed from left to right.*

6 Summary

In this paper we describe the method of [3], which is a refinement of the approach developed in [2], for attenuation correction in Fluorescence Confocal Microscopy using Fast Fourier Transform methods. This approach, valid for weak attenuation, consists in multiplying the measured fluorescent intensity by a correction factor involving a convolution integral of the measured signal, which can be computed efficiently by an FFT-based algorithm. By a statistical reformulation of the problem it is possible to derive

first order moment and cumulant estimators leading to a nonlinear integral equation for the unknown fluorescent density, which can be solved by an iterative method. In each iteration the convolution of the previous estimate is computed by means of the FFT. The first iterate of the new estimators coincides with the approximation used in [2] for very weak attenuation. It turns out that the moment estimator with two iterations gives the best results, which are more accurate than the layer method of [4]. Since only two iterations are needed, the advantage in computational efficiency over the layer method is retained. We conclude therefore that the combined results of [2] and [3] provide an efficient and accurate method for attenuation correction in confocal microscopy.

References

[1] Ortega J.M. and W.C. Rheinboldt (1970). *Iterative Solution of Nonlinear Equations in Several Variables*. Ac. Press, New York.

[2] Roerdink J.B.T.M. and M. Bakker (1993). An FFT-based method for attenuation correction in fluorescence confocal microscopy. J. Microscopy 169, 3–14.

[3] Roerdink J.B.T.M. (1994). FFT-based methods for nonlinear image restoration in confocal microscopy, J. Math. Imaging and Vision 4(2), 199–207.

[4] Visser T.D., F.C.A. Groen and G.J. Brakenhoff (1991). Absorption and scattering correction in fluorescence confocal microscopy. *J. Microscopy* 163, 189-200.